Available online at www.sciencedirect.com
ScienceDirect
Journal of Molecular Catalysis A: Chemical 285 (2008) 120–127
JOURNAL OF MOLECULAR CATALYSIS A: CHEMICAL
www.elsevier.com/locate/molcata

Quantum chemical determination of stable intermediates for alkene epoxidation with Mn-porphyrin catalysts

María C. Curet-Arana, Gloria A. Emberger, Linda J. Broadbelt *, Randall Q. Snurr **

Department of Chemical and Biological Engineering, Northwestern University, 2145 Sheridan Road Evanston, IL 60208-3120, USA

Received 5 July 2007; received in revised form 18 January 2008; accepted 21 January 2008
Available online 6 February 2008

Abstract

Density functional theory (DFT) and hybrid quantum mechanics/molecular mechanics (QM/MM) calculations were used to study stable intermediates for alkene epoxidation using Mn-porphyrin catalysts. For the reaction intermediate involving complexation of the alkene with the oxidized Mn-porphyrin, four intermediates have been proposed in the literature. A concerted mechanism with no intermediate has also been proposed, and these five mechanisms could all involve the formation of a product complex. Our calculations show that the product complex has the lowest energy, followed by the radical intermediate. The metallaoxetane intermediate is much higher in energy, and the calculations do not support carbocation or pi-radical cation intermediates. A polarizable continuum model was used to account for solvent effects, and the calculated energies of solvation are comparable for all minima along the reaction path.

Keywords: Metalloporphyrin; Epoxide; Propene; Styrene; Reaction pathway; Density functional theory

1. Introduction

There is a strong interest in Mn-porphyrins as catalysts for epoxidation reactions due to the similarity of these catalysts to cytochrome P-450 enzymes, which perform oxidation reactions in living systems. Mn-porphyrins, such as 5,10,15,20-tetraphenyl porphyrinato manganese (III) chloride (MnTPP-Cl), have been extensively used to mimic this enzyme. Although these porphyrins can catalyze epoxidation reactions, two major limitations have arisen. First, Mn-porphyrins are easily deactivated due to μ-oxo dimer formation. Second, they do not provide good reactant selectivity. In the past few decades efforts have been made to improve the stability of these catalysts, and reviews by Jacobsen and Meunier provide comprehensive summaries of Mn-porphyrin catalysts and modifications that have been made to induce stability and selectivity [1,2]. In general, there have been two common approaches to improve Mn-porphyrin catalysts. In the first approach, bulky side groups are attached to the sides of the porphyrin to prevent the formation of μ-oxo dimmers [3–5]. In the second approach, porphyrins have been immobilized on solid supports, such as silica, to improve their stability [6–8]. Recently, Hupp, Nguyen and co-workers have demonstrated a third approach, in which Mn-porphyrins are encapsulated in self-assembling nanocavities known as molecular squares [9–11]. This encapsulation was shown to prevent deactivation and induce reactant selectivity for 2,8,12,18-tetrabutyl-3,7,13,17-tetramethyl-5,15-bis(4-pyridyl)porphyrinato manganese (III) chloride (MnDPyP).

The catalytic cycle shown in Fig. 1 is commonly accepted as the basic mechanism for epoxidation reactions with Mn-porphyrins. However, despite extensive research, some details of the mechanism are still not known, particularly the nature of the intermediates. The catalytic cycle in Fig. 1 involves two important intermediates: the oxidized Mn-porphyrin and the intermediate that is formed when the alkene binds to the oxidized porphyrin. Metal-oxo species (Mn=O) have been suggested most frequently as the form of the oxidized porphyrin involved in epoxidation [2,12], and recent experimental work supports this idea. Groves and co-workers generated a water-soluble oxidized Mn-porphyrin with *m*-chloroperoxybenzoic acid (*m*-CPBA), HSO_5^- (oxone) and OCl^- at room temperature and in aqueous solution, and they were able to obtain a ^{1}H NMR

* Corresponding author. Tel.: +1 847 491 5351; fax: +1 847 491 3728.
** Corresponding author. Tel.: +1 847 467 2977; fax: +1 847 467 1018.
E-mail addresses: broadbelt@northwestern.edu (L.J. Broadbelt), snurr@northwestern.edu (R.Q. Snurr).

1381-1169/$ – see front matter © 2008 Elsevier B.V. All rights reserved.
doi:10.1016/j.molcata.2008.01.036

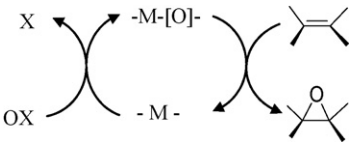

Fig. 1. Schematic diagram of the catalytic cycle for the epoxidation of an alkene using a Mn-porphyrin. Oxygen is transferred first from the oxidant to the metal and then to the alkene to form the epoxide.

spectrum that supports the Mn-oxo species [13–15]. However, this oxidized Mn-porphyrin created by Groves and co-workers is unreactive with alkenes. Studies on the closely related Mn(salen) system, which catalyzes epoxidation reactions with high enantioselectivity, have shown that the Mn-oxo species exists and is reactive with olefins and sulfides [16]. In particular, Feichtinger and Plattner used electrospray mass spectrometry (ESMS) to detect the Mn-oxo species formed when iodosylbenzene (PhIO) and bleach were used as oxidants. They also detected these complexes in the presence of N-oxide axial ligands [17]. Recent investigations performed by Goldberg and co-workers suggest a different form for the active epoxidation catalyst [18]. They propose that the active catalyst is formed when a second oxidant molecule (XO) is bound to the oxidized porphyrin (Mn=O). A third epoxidizing intermediate has also been postulated for both Mn(salen) and Fe-porphyrin systems. The *cis*/*trans* ratios of the epoxidation products formed using either of these two catalyst systems were found to be dependent on the oxidant used [19–21], and this dependence was explained by proposing that the oxidant forms an adduct with the metal center and directly epoxidizes the substrate. Only the Mn-oxo species was investigated in the present study because it is commonly accepted to be the active intermediate. Since the main cause of deactivation is formation of μ-oxo dimers,

$$M{=}O + M \leftrightarrow M{-}O{-}M \quad (1)$$

the identity and nature of the active catalytic species can have significant implications on deactivation, as well as reaction kinetics.

For the complexation of the alkene with the oxidized porphyrin, four intermediates have been proposed in the literature, as well as a concerted mechanism that leads directly to a product complex [22–27]. These intermediates, shown in Fig. 2,

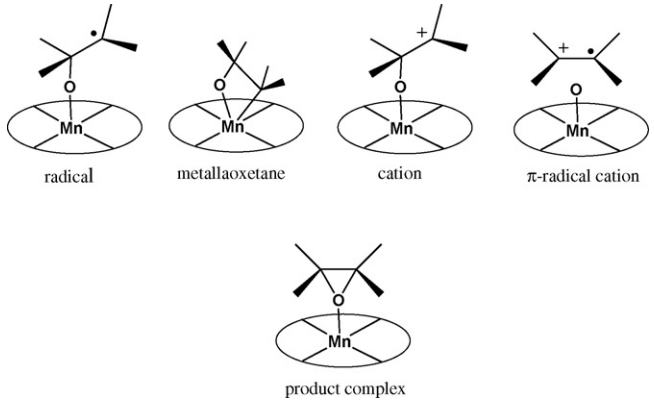

Fig. 2. Proposed intermediates for the alkene complexed with the oxidized porphyrin.

have been proposed based on reaction kinetics and selectivities, and there is no direct evidence for which of these intermediates participates in the reaction mechanism. As a complement to experimental studies, quantum mechanical (QM) calculations can be used to analyze the stability and reactivity of these intermediates. In particular, density functional theory (DFT) and hybrid QM/molecular mechanics (MM) methods are tractable, depending on the size of the porphyrin and alkene of interest. In QM/MM, DFT is used only for a central region where the important chemistry occurs, and the surrounding atoms are treated with a classical force field. These combined QM/MM approaches thus have the potential to provide DFT-level predictions for very large systems, for example porphyrins encapsulated in molecular squares or other environments.

In contrast to iron porphyrins, a small number of papers involving QM calculations of Mn-porphyrins have been published. For example, Liao et al. recently reported DFT calculations on unligated and ligated Mn-porphyrins with pyridine as the ligand [28]. In some studies of Mn-porphyrins a planar conformation of the porphyrin ring has been assumed. Quantum mechanical calculations of the oxidized manganese porphyrin have been carried out as well. One of the first modeling studies to elucidate the electronic structure of an oxidized manganese porphyrin was by Zwaans et al. [29]. The level of theory for their calculations was based on a closed-shell Hartree Fock method with a fairly low-level STO3G basis set. More recently, Ghosh et al. reported molecular structures for the oxidized forms of manganese and iron porphyrins using DFT calculations [30,31]. The work of Ghosh and Gonzalez [31] focused on high-valent manganese-oxo species of the form $[(P)Mn(O)Y]^{0,-1}$, where P = tetramesityl porphyrin and Y = F, PF_6, and $[(P)Mn(O)(Py)]^{+1,0}$, where Py = pyridine, and comprehensively mapped the energetics and electronic distributions. De Angelis et al. [32] also studied oxomanganese (V) porphyrins of the form dioxo, oxo-hydroxy or oxo-aqua and characterized the relative energetics of the singlet, triplet and quintet spin states, and de Visser et al. [33] compared Mn-porphyrin and Mn-corrole complexes using DFT to understand differences in their reactivity.

A large number of computational studies on the similar Mn(salen) system has been performed, offering insight into the mechanism of Mn-porphyrin systems. Most of the studies use a model representation of the Mn(salen) complex although a few studies of the full Mn(salen) complex have shown that the smaller model gives reasonable results [34–36]. Strassner and Houk [37] examined model neutral and cationic Mn(salen) and oxo-Mn(salen) species using DFT methods in an effort to order the spin states. More extensive studies have investigated the entire reaction path. Several post-Hartree Fock methods have been used to try to elucidate the spin state ordering of the Mn(salen), oxo-Mn(salen), and various intermediate species and to determine the appropriate functional to use for DFT studies [38–40]. Generally, pure DFT functionals gave better qualitative agreement with the post-Hartree Fock calculations than the hybrid functionals. Cavallo and Jacobsen demonstrated that the choice of functional gives qualitatively different reaction paths [41]. Several studies showed spin conservation along the triplet

surface is possible when the BP86 functional is used while B3LYP results support spin crossing to the quintet surface when a radical intermediate is formed [41,42]. Cavallo and Jacobsen [34] calculated the activation barrier for the concerted pathway to be higher than that for the radical pathway and therefore showed a radical intermediate to be likely. Morokuma and co-workers [43] have investigated the mechanism of epoxidation with peracetic acid as the oxidant with a variety of axial ligands. Their results indicated that the reaction along the quintet surface can occur in a concerted fashion with imidazole as the axial ligand while a stepwise mechanism proceeding through a radical intermediate is likely for other complexes and spin states. Another study illustrated that the axial ligands CH_3CN and $ON(CH_3)_3$ decrease the triplet-quintet gap and may explain the experimentally observed increase in rate in the presence of the ligands [44]. This study also found that the ligands induced folding of the salen ligand into a stepped or cupped configuration. Cavallo and Jacobsen [35] also correlated geometrical parameters and Mn–O bond strengths to electronic effects of substituents on the Mn(salen).

To the best of our knowledge, there have been no previous DFT studies of alkene complexes with oxidized Mn-porphyrins. To fill this void, we used DFT and QM/MM calculations to investigate proposed intermediates for the epoxidation of alkenes with a Mn-porphyrin catalyst. The main focus of the calculations was the stability and reactivity of the proposed alkene/oxidized porphyrin intermediates. The transition states (TS) and the full reaction path for various intermediates are discussed in a separate study [45]. Different spin multiplicities were examined, as well as the effect of a surrounding solvent. The results obtained here along with the TS results presented elsewhere support two of the proposed intermediates for the alkene/oxidized porphyrin complex but not the other three proposed intermediates. In addition, we carried out our own study of the oxidized Mn-porphyrin to calculate the energetic requirements to form the different alkene/oxidized porphyrin intermediates. To complete the catalytic cycle shown in Fig. 1, we also calculated the geometry and energetics of the bare Mn-porphyrin.

2. Methodology

Spin-unrestricted DFT calculations were performed to obtain optimized geometries for the manganese porphyrin and stable intermediates along the reaction coordinate for epoxidation of propene and styrene. The specific Mn-porphyrin analyzed is shown in Fig. 3 (left). It is a mimic of MnTPP that has been studied in previous experiments for epoxidation reactions [46,47]. All calculations were carried out with the Gaussian 98 program package unless otherwise noted [48]. Unrestricted PW91 GGA was used as the exchange-correlation functional [49,50]. Although CCSD(T) calculations on the Mn(salen) system have shown that both pure and hybrid functionals fail to predict spin-state ordering reliably [38], the choice of PW91 here was validated because it has been shown to correctly reproduce the singlet ground state of Mn(V)O porphyrins [30–32,51]. The effective core potential LANL2DZ was used as the basis set. This is a double-ζ quality Dunning basis set that replaces core

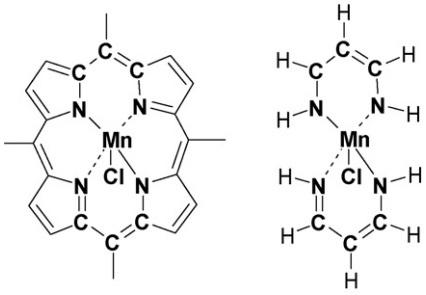

Fig. 3. The porphyrin studied in this work (left). The left hand structure shows the atoms included in the inner layer ONIOM partitioning with their atomic symbols and atoms in the outer layer with a stick representation. As shown on the right, the inner layer was capped with hydrogen link atoms for the high-level DFT calculations in the ONIOM approach.

electrons with a potential field to save computational cost. Additional test calculations using a larger basis set provided similar results (See Supporting Information).

An integrated QM/MM method was also used in parallel with the full DFT calculations. The QM/MM calculations were carried out using the ONIOM approach with mechanical embedding as implemented in Gaussian 98 [52–55]. For the ONIOM calculations the system was divided into two layers: the inner layer, which was analyzed with DFT as described above, and the outer layer, which was analyzed with the UFF force field [56]. Fig. 3 shows the inner and outer layers that were used for the Mn-porphyrin, as well as the hydrogen link atoms that were used when a bond was cut for the partitioning between the inner and outer layers. Mohr et al. [57] showed that this partitioning scheme was better able to reproduce the relative energies of the different spin states for Fe porphyrins than one that included the two additional carbon atoms in the central region. The energies of iodosylbenzene and phenyl iodide were calculated using full DFT, and they were included in the inner layer of the ONIOM calculations. For the oxidized porphyrin, the oxygen atom was also included in the inner layer. The propene system was analyzed using both full DFT and ONIOM; for the reaction of styrene, only ONIOM calculations were performed. In the ONIOM calculations, the entire propene molecule was included in the inner layer. For the styrene complexes, the phenyl ring was treated with the low level, and the other styrene atoms were assigned to the high level. Single-point energy calculations in which the entire styrene molecule was included in the high level were performed on the optimized styrene complexes with the Gaussian 03 program package [58]. These calculations gave the same qualitative results as those where the phenyl ring was assigned to the low level, validating the partitioning scheme used for the calculations involving styrene.

Geometries and energies were obtained by performing full geometry optimization with no symmetry constraints. The optimization of stable species was verified with frequency calculations for both the DFT and ONIOM methods, and wavefunction stability was confirmed [59,60]. Energies were corrected for basis set superposition error with the counterpoise method [61]. Natural bond order (NBO) analysis was performed for all intermediates. Standard statistical mechanics was used

Table 1
Relative energies in kJ mol^{-1} of Mn-porphyrin intermediates

Molecule	Method	Singlet	Triplet	Quintet
Mn-porphyrin	DFT	80	51	0
	ONIOM	102	47	0
Oxidized Mn-porphyrin	DFT	0	1	29
	ONIOM	0	4	24
Propene product complex	DFT	65	13	0
Propene product complex	ONIOM	–	13	0
Styrene product complex	ONIOM	84	0	9
Propene radical intermediate	DFT	N/A	8	0
Propene radical intermediate	ONIOM	N/A	50	0
Styrene radical intermediate	ONIOM	N/A	1	0

Each row is referenced to its own lowest spin state. N/A, not applicable; –, calculation was not performed.

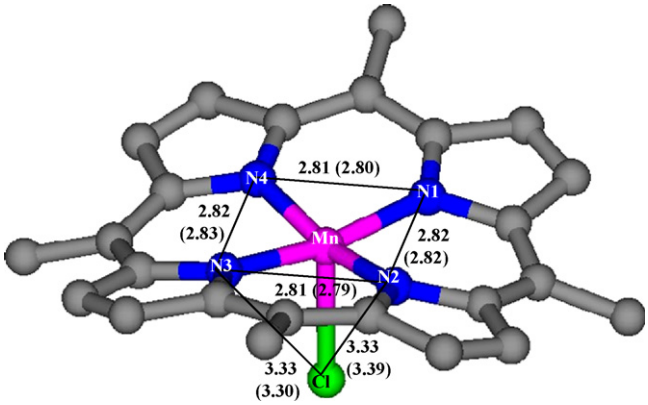

Fig. 4. Comparison of bond lengths (Å) for the optimized quintet Mn-porphyrin and the crystal structure of MnTPP-Cl. Crystal structure lengths are shown in parenthesis [63].

to calculate the translational, vibrational, rotational, and electronic contributions to the partition function. The rigid-rotor, harmonic-oscillator approximation was used to obtain the vibrational frequencies. A polarizable continuum model (PCM) was used to study solvent effects on the energies of the stable intermediates. For these calculations, dichloromethane was used as the solvent, which has a dielectric constant of 8.93.

3. Results

This section first presents an analysis of the Mn-porphyrin and the oxidized Mn-porphyrin. These analyses provide the opportunity to compare calculated quantities to experimental and other theoretical values reported in the literature. We also present a detailed comparison of results from QM/MM versus full DFT. Next, results for the four proposed alkene/oxidized porphyrin intermediates and the product complex are presented. Propene and styrene were chosen as the alkenes. With the exception of species involving styrene, all species were analyzed with both ONIOM and DFT to test the QM/MM method. Based on good agreement of the ONIOM and full DFT results for propene, the styrene calculations were performed only with ONIOM. Various possible spin multiplicities were considered in all cases. Reaction participants were considered first in vacuum, and solvent effects are described at the end of the section.

3.1. Mn-porphyrin

Minimum-energy structures of the Mn-porphyrin were determined for singlet, triplet and quintet spin states. Both ONIOM and DFT predict that the quintet is the lowest energy state. As shown in Table 1, the triplet state is about 50 kJ/mol higher in energy, and the singlet state is more than 80 kJ/mol higher in energy than the quintet state. Krzystek et al. analyzed Mn-porphyrins using high-frequency and high-field electron paramagnetic resonance and also found that the quintet state is the lowest energy state [62].

The optimized structure for the quintet Mn-porphyrin is shown in Fig. 4. The predicted bond lengths are in very good agreement with those from the crystal structure of MnTPP-Cl [63], as indicated in the figure. A non-planar conformation is observed both in experiment and in the calculated structure. Tulinsky and Chen [63] report that the Mn atom is displaced 0.27 Å with respect to the plane formed by the nitrogen atoms. Both ONIOM and DFT results are in good agreement with this observation, with predicted displacements of 0.25 and 0.26 Å, respectively.

Spin densities, charges, and the electronic configuration of the Mn atom were calculated for the triplet and quintet states. All quantities agree well between ONIOM and full DFT. (See Supporting Information). For both the triplet and quintet states, the 4s orbital of Mn is mostly unoccupied, and the unpaired electrons are mainly localized on the 3d orbitals of Mn. This is in agreement with the electron spin distribution published by Turner and Gunter from ^{13}C NMR spectroscopy [64].

3.2. Oxidized Mn-porphyrin

For the oxidized Mn-porphyrin, both DFT and ONIOM predict that the singlet and triplet states are almost degenerate, with a slight preference for the singlet state as shown in Table 1. The quintet state is approximately 25 kJ/mol higher in energy. Both high and low spin oxidized Mn-porphyrins have been detected experimentally [13–15,65]. While the Mn-porphyrins studied in the experimental work are not exactly the same as the one used in the calculations, they suggest that both singlet and triplet states are plausible states for oxidized Mn-porphyrins. This relative ranking is also consistent with the DFT calculations of De Angelis et al. [32], who observed $E_{\text{singlet}} < E_{\text{triplet}} < E_{\text{quintet}}$ for all oxo-Mn-porphyrins that they studied, and with the CASSCF calculations of Sears and Sherrill [40] performed on an oxo-Mn(salen) complex.

The optimized geometry from the calculations is shown in Fig. 5. The oxidized porphyrin maintains its ruffled conformation, but the Mn atom is shifted up 0.4 Å in the z-direction compared to the Mn-porphyrin. The ONIOM and DFT structures are very similar (See Table S5). From DFT, the Mn–O bond length is 1.60 Å for the singlet spin state and 1.66 Å for the triplet state, in good agreement with the experimental value of 1.69 Å found by Ayougou et al. [65]. Czernuszewicz et al. mea-

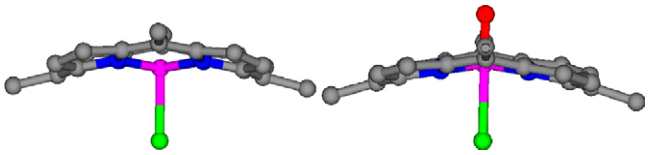

Fig. 5. Optimized structure for the Mn-porphyrin (left) and the oxidized Mn-porphyrin (right).

sured the stretching frequency of Mn–O in high-spin oxidized Mn-tetramesitylporphyrin using resonance Raman and infrared spectroscopies [66]. Their value, 754 cm^{-1}, is in reasonable agreement with the frequency of our high spin oxidized porphyrin as shown in Table 2. Similarly, Collins et al. detected the stretching frequency of Mn–O for a low-spin Mn-oxo complex [67]. The reported frequency, 979 cm^{-1}, is comparable with the Mn–O frequency of our calculations for the low-spin case (Table 2). An NBO analysis reveals that the Mn–O bond has double bond character. By performing a molecular orbital overlap population analysis, it was found that the Mn d_{xz}–O p_x and Mn d_{yz}–O p_y orbitals have the highest overlap. The results indicate that the Mn–O bond has some triple bond character, and the double bond can therefore be described as a resonance between a single and triple bond.

3.3. Alkene/Mn-porphyrin intermediates

Calculations were performed to analyze the five structures shown in Fig. 2, which are formed assuming that the Mn-oxo species is the active catalyst (Fig. 1) as is most commonly accepted. Starting from different initial configurations, geometry optimizations yielded stable product complexes and radical intermediates for propene (both full DFT and ONIOM) and styrene (ONIOM). A high energy metallaoxetane structure was also found for styrene. Mulliken and NBO charges were calculated for all of the intermediates. None of the structures found in our calculations showed a positive charge on the C_2 atom, as required for the proposed cation and pi-radical cation intermediates. The calculations do not definitively rule out these intermediates, because, for example, they might be stabilized by solvents which are neglected in these calculations. However, Bruice and co-workers [26] rule out a mechanism involving rate-limiting formation of an alkene-derived π-radical cation based on substituent effect and electron transfer arguments. A cationic intermediate was also ruled out for the Mn(salen) system by Adam et al. [19], who found no cationic ring-opening products when using the probe molecule (1α,2β,3α)-(2-ethenyl-3-methoxycyclopropyl)benzene in an epoxidation reaction. The relative energies of the intermediates formed with styrene and propene and their geometries are shown in Fig. 6. For both propene and styrene, the product complex is the lowest energy configuration. When the reactant is propene, the radical intermediate is 40 kJ/mol higher in energy. ONIOM is in very good agreement with DFT. For styrene, the difference between the radical intermediate and the product complex is 26 kJ/mol for the quintet state, and the metallaoxetane intermediate with the phenyl ring in the proximal position (singlet) is about 150 kJ/mol higher in energy than the radical.

Table 1 shows the difference in energy between spin states for the propene and styrene intermediates. For the propene product complex, the quintet state has the lowest energy, and the triplet state is 13 kJ/mol higher in energy for both DFT and ONIOM calculations. For styrene, ONIOM predicts that the triplet state is lower in energy than the quintet state, with an energy gap of 9 kJ/mol. The optimized geometry for the product complex with styrene as obtained with ONIOM is shown in Fig. 7 (right). In the product complex, the Mn–O interaction is very weak. For the propene and styrene intermediates in the triplet state, the Mn–O bond is 2.1 Å, while for the quintet spin state, the separation between both atoms is even longer (2.7 Å). For both systems, the O–C_1 and O–C_2 bond lengths are very similar to the bond lengths of the epoxide (Table S5). For the triplet and quintet spin states, the unpaired electrons are mainly localized on the Mn atom. Even though the interaction between Mn and O is very weak and the O–C bond distances are very close to the values in the epoxide, the charge and the spin density of the Mn atom in this intermediate are lower than the values obtained for the bare Mn-porphyrin at these multiplicities, indicating that it is a true intermediate.[1] A molecular orbital overlap population analysis showed that the Mn–O bond is mainly formed with the Mn p_z orbital.

For the radical intermediate, DFT and ONIOM predict that the quintet state is the lowest energy state for the propene and styrene systems (Table 1). Cavallo and Jacobsen also found the quintet state to be the lowest energy state for the radical intermediate in their DFT studies on Mn(salen)-catalyzed epoxidation reactions [41,68]. However, a quantitative discrepancy between the two computational methods was obtained for the propene intermediate. For this system, DFT predicts that the triplet state is 8 kJ/mol higher in energy than the quintet state, whereas ONIOM predicts that the difference is 50 kJ/mol. This large discrepancy is consistent with the unusually low value of the spin density on Mn for the ONIOM calculation of the triplet state, which was substantially different from the DFT value, even though spin contamination was not present in either case. For styrene the triplet and the quintet states are almost degenerate, with a difference of 1 kJ/mol between both spin states. The spin density on Mn from the ONIOM calculations of the styrene radical intermediate was similar to those for the radical intermediate of propene from DFT, indicating that this energy difference is more reasonable than the one obtained for the ONIOM calcu-

Table 2
Stretching frequencies for the Mn—O bond

	DFT (cm^{-1})	ONIOM (cm^{-1})	Experimental value (cm^{-1})
ν_{Mn-O} low spin	913	930	979[a]
ν_{Mn-O} high spin	796	783	754[b]

[a] From Collins et al. [67].
[b] From Czernuszewicz et al. [66].

[1] Note that in Ref. [45], we refer to the product complex as the "concerted intermediate" for this reason.

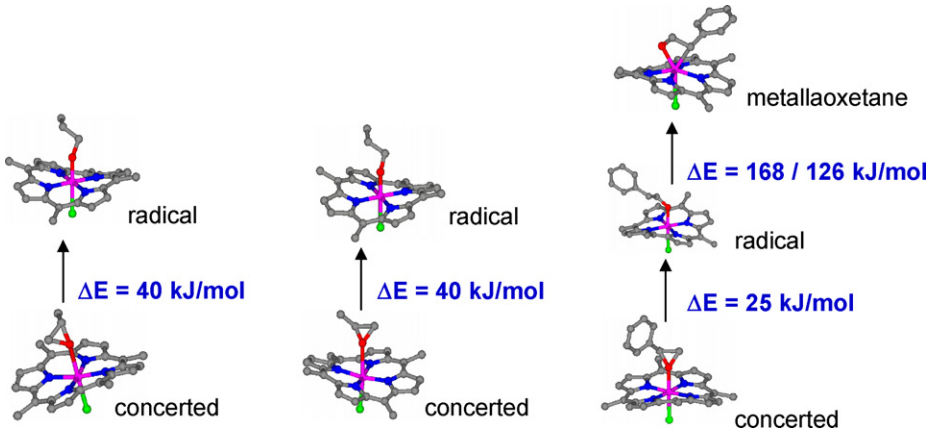

Fig. 6. Relative energies between intermediates as obtained with DFT and ONIOM. "Concerted" indicates the product complex, which plays a key role in the concerted mechanism. Results are shown for the quintet spin state for all species except the metallaoxetane, for which only a single state was found. (The results for the propene intermediate were obtained with Gaussian 98 [48] while the results for the styrene intermediate were obtained with Gaussian 03 [58].) For the energy differences between the radical and metallaoxetane intermediates, the first energy difference is for the metallaoxetane where the phenyl ring is in the proximal position, as shown in the figure. The second energy difference is for the metallaoxetane with the phenyl ring in the distal position.

lations for propene. Fig. 7 (left) illustrates the geometry for the styrene radical intermediate. The Mn–O bond is longer than for the oxidized porphyrin, with a bond length greater than 1.8 Å at all multiplicities. For the Mn–O bond in this intermediate, the interaction between Mn d_{xz} and O p_x, which was observed in the oxidized Mn-porphyrin, diminishes, and the bond is mainly formed with the Mn d_{yz} and O p_y orbitals. The C_1–C_2 bond in this intermediate (1.5 Å) is also much longer than the double bond of propene (1.36 Å). At this point, the double bond of propene has already changed character, and there is a single bond between C_1 and C_2. In this intermediate, the geometries obtained for the triplet and quintet states are almost identical. The unpaired electrons are mainly localized on the Mn atom and on the C_2 atom, with a small contribution from the oxygen atom. However, the main difference between the two spin states is the spin density on the C_2 atom. For the triplet state, C_2 has a spin down electron, while for the quintet state it has a spin up electron. For the formation of the radical intermediate there is a slight charge transfer between the oxidized porphyrin and the alkene of 0.3 electrons, which was observed in the triplet and quintet states with both ONIOM and full DFT.

3.4. Reaction intermediates and solvent effects

In order to obtain a better understanding of the reaction mechanism, energy differences between intermediates were compared for the epoxidation of propene. Fig. 8 illustrates the relative electronic energies for different intermediates obtained with DFT and ONIOM when iodosylbenzene is used as the oxidant. The solid line corresponds to the DFT results and the triangles correspond to ONIOM results. We have mapped the transition states for the reaction of styrene using ONIOM, as described elsewhere [45]. Here we focus on the plateaus that represent the energies of the lowest energy states of each intermediate for propene and a comparison between ONIOM and DFT. Energies for the radical intermediate and product complex were corrected for basis set superposition error with the counterpoise method [61]. The overall reaction is exothermic, with a $\Delta E_{reaction}$ close to −250 kJ/mol. Each of the elementary steps is also exothermic. The oxidation of the porphyrin (state I to state II) has a $\Delta E_{reaction}$ close to −190 kJ/mol. The binding of styrene to form the radical intermediate (state II to state III_r) and to form

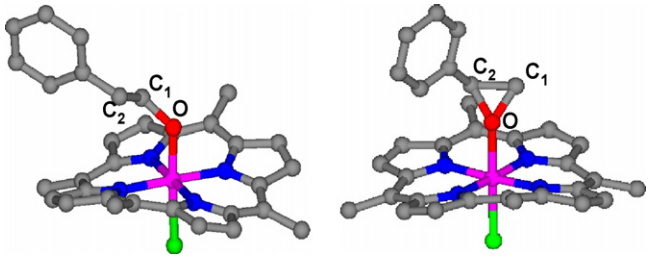

Fig. 7. Geometries for radical intermediate (left) and product complex (right) with styrene in the triplet spin state obtained using ONIOM.

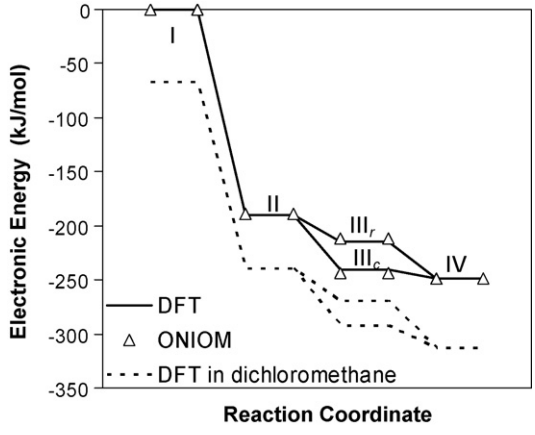

Fig. 8. Energy diagram for the epoxidation of propene. Comparison between DFT, ONIOM and PCM is shown. The first state (I) consists of the Mn-porphyrin, iodosylbenzene and propene. State II is the oxidized porphyrin, phenyl iodide and propene. State III_r is the radical intermediate and phenyl iodide, and state III_c is the product complex and phenyl iodide. The fourth state (IV) is the Mn-porphyrin, propene oxide and phenyl iodide.

the product complex (state II to state III_c) are both exothermic, with $\Delta E_{reaction}$ close to −22 and −55 kJ/mol, respectively. The formation of styrene oxide from either the product complex (state III_c to state IV) or from the radical intermediate (state III_r to state IV) is also downhill. As seen from this figure, the ONIOM results match the full DFT results very well. For instance, in states III_r and III_c the difference between DFT and ONIOM is less than 3 kJ/mol, and for states I, II and IV the difference is approximately 1 kJ/mol. The role of the different intermediates in leading to the observed reaction products for the case of styrene is discussed in Ref. [45]. The focus of the current study is to determine stable reaction intermediates, which is one important factor in determining their relative importance in the mechanism.

A polarizable continuum model was used to study the effect of the solvent on the energies of the stable intermediates. For these calculations, dichloromethane was used as the solvent. Single-point calculations were performed with and without PCM using PW91/LANL2DZ on the optimized structures obtained in vacuum from ONIOM. Optimization with PCM on the bare Mn-porphyrin did not lower the energy significantly compared to the single-point calculation with PCM, and changes in the geometry between vacuum and PCM results were negligible. No significant differences in atomic charges or spin densities were obtained when the solvent was taken into account for any of the species. In the presence of solvent, as in the vacuum results, the product complex is lower in energy than the radical intermediate, and Fig. 8 illustrates the relative energies for the reaction intermediates for propene epoxidation in the presence of the solvent with the Mn-porphyrin catalyst. When the solvent is taken into account, the differences in energy among the intermediates remain essentially the same as in vacuum, and the topology of the energy diagram does not change. Energies of solvation obtained were comparable for all species at a value of approximately 57 kJ/mol. Although the effect of the solvent was not large in this study, it can be expected that solvent effects on the cationic Mn-porphyrin would be significant.

4. Conclusions

Proposed intermediates in the epoxidation of alkenes with Mn-porphyrin catalysts have been investigated using DFT and hybrid QM/MM (ONIOM) calculations. In general, the ONIOM results are in very good agreement with those from full DFT calculations. Spin densities, atomic charges, electronic configurations, geometries and relative energies between spin states are similar for DFT and ONIOM for all stable intermediates. For the reaction intermediate where the alkene is complexed with the oxidized Mn-porphyrin, our calculations suggest that the product complex has the lowest energy and the radical intermediate is also reasonable. The metallaoxetane is much higher in energy, and the proposed carbocation and pi-radical cation intermediates are not supported by these calculations. These findings support either a concerted or radical mechanism. A study of the full reaction coordinate is needed to determine which pathway is more likely [45].

Acknowledgments

This research is supported by the Chemical Sciences, Geosciences, and Biosciences Division, Office of Basic Energy Sciences, Office of Science, U.S. Department of Energy, Grant No. DE-FG02-03ERIS457, the National Science Foundation (CTS-0507013), the Illinois Minority Graduate Incentive Program (MCC), and the National Defense Science and Engineering Graduate Fellowship Program (GAE). The authors thank Profs. SonBinh Nguyen and Joseph Hupp for helpful discussions and an anonymous referee for helpful comments.

Appendix A. Supplementary data

Supplementary data associated with this article can be found, in the online version, at doi:10.1016/j.molcata.2008.01.036.

References

[1] E. Jacobsen, in: G. Wilkinson, F. Stone, E. Abel, L. Hegedus (Eds.), Comprehensive Organometallic Chemistry II, Pergamon, 1995, p. 1097.
[2] B. Meunier, Chem. Rev. 92 (1992) 1411–1456.
[3] A.N. de Sousa, M. de Carvalho, Y.M. Idemori, J. Mol. Catal. A-Chem. 169 (2001) 1–10.
[4] M.C. Feiters, A.E. Rowan, R.J.M. Nolte, Chem. Soc. Rev. 29 (2000) 375–384.
[5] M.L. Merlau, W.J. Grande, S.T. Nguyen, J.T. Hupp, J. Mol. Catal. A-Chem. 156 (2000) 79–84.
[6] H.C. Sacco, Y. Iamamoto, J.R.L. Smith, J. Chem. Soc.-Perkin Trans. 2 (2001) 181–190.
[7] F.G. Doro, J.R.L. Smith, A.G. Ferreira, M.D. Assis, J. Mol. Catal. A-Chem. 164 (2000) 97–108.
[8] P.E.F. Neys, A. Severeyns, I.F.J. Vankelecom, E. Ceulemans, W. Dehaen, P.A. Jacobs, J. Mol. Catal. A-Chem. 144 (1999) 373–377.
[9] S.T. Nguyen, D.L. Gin, J.T. Hupp, X. Zhang, Proc. Natl. Acad. Sci. U.S.A. 98 (2001) 11849–11850.
[10] P.H. Dinolfo, J.T. Hupp, Chem. Mater. 13 (2001) 3113–3125.
[11] M.L. Merlau, M.D.P. Mejia, S.T. Nguyen, J.T. Hupp, Angew. Chem.-Int. Ed. 40 (2001) 4239–4242.
[12] M.J. Gunter, P. Turner, Coord. Chem. Rev. 108 (1991) 115–161.
[13] J.T. Groves, J.B. Lee, S.S. Marla, J. Am. Chem. Soc. 119 (1997) 6269–6273.
[14] N. Jin, J.L. Bourassa, S.C. Tizio, J.T. Groves, Angew. Chem.-Int. Ed. 39 (2000) 3849–3851.
[15] N. Jin, J.T. Groves, J. Am. Chem. Soc. 121 (1999) 2923–2924.
[16] D. Feichtinger, D.A. Plattner, Angew. Chem.-Int. Ed. 36 (1997) 1718–1719.
[17] D.P.D.A. Feichtinger, Chem.: Eur. J. 7 (2001) 591–599.
[18] S.H.L. Wang, B.S. Mandimutsira, R. Todd, B. Ramdhanie, J.P. Fox, D.P. Goldberg, J. Am. Chem. Soc. 126 (2004) 18–19.
[19] W. Adam, K.J. Roschmann, C.R. Saha-Moller, D. Seebach, J. Am. Chem. Soc. 124 (2002) 5068–5073.
[20] J.P. Collman, L. Zeng, J.I. Brauman, Inorg. Chem. 43 (2004) 2672–2679.
[21] W. Nam, S.W. Jin, M.H. Lim, J.Y. Ryu, C. Kim, Inorg. Chem. 41 (2002) 3647–3652.
[22] J.P. Collman, J.I. Brauman, P.D. Hampton, H. Tanaka, D.S. Bohle, R.T. Hembre, J. Am. Chem. Soc. 112 (1990) 7980–7984.
[23] J.P. Collman, J.I. Brauman, B. Meunier, T. Hayashi, T. Kodadek, S.A. Raybuck, J. Am. Chem. Soc. 107 (1985) 2000–2005.
[24] R.J.M. Nolte, A.S.J. Razenberg, R. Schuurman, J. Am. Chem. Soc. 108 (1986) 2751–2752.
[25] J. Razenberg, A.W. Vandermade, J.W.H. Smeets, R.J.M. Nolte, J. Mol. Catal. 31 (1985) 271–287.
[26] R.D. Arasasingham, G.X. He, T.C. Bruice, J. Am. Chem. Soc. 115 (1993) 7985–7991.

[27] G.X. He, R.D. Arasasingham, G.H. Zhang, T.C. Bruice, J. Am. Chem. Soc. 113 (1991) 9828–9833.
[28] M.S. Liao, J.D. Watts, M.J. Huang, Inorg. Chem. 44 (2005) 1941–1949.
[29] R. Zwaans, J.H. Van Lenthe, D.H.W. den Boer, in: P.W.N. Van Leeuwen (Ed.), Theoretical Aspects of Homogeneous Catalysis, Kluwer Academic Publishers, 1995, p. 197.
[30] A. Ghosh, T. Vangberg, E. Gonzalez, P. Taylor, J. Porphyrins Phthalocyanines 5 (2001) 345–356.
[31] A. Ghosh, E. Gonzalez, Isr. J. Chem. 40 (2000) 1–8.
[32] F. De Angelis, N. Jin, R. Car, J.T. Groves, Inorg. Chem. 45 (2006) 4268–4276.
[33] S.P. de Visser, F. Ogliaro, Z. Gross, S. Shaik, Chem.: Eur. J. 7 (2001) 4954–4960.
[34] L. Cavallo, H. Jacobsen, Angew. Chem.-Int. Ed. 39 (2000) 589–592.
[35] L. Cavallo, H. Jacobsen, J. Org. Chem. 68 (2003) 6202–6207.
[36] I.V. Khavrutskii, D.G. Musaev, K. Morokuma, Inorg. Chem. 42 (2003) 2606–2621.
[37] T. Strassner, K.N. Houk, Org. Lett. 1 (1999) 419–422.
[38] Y.G. Abashkin, J.R. Collins, S.K. Burt, Inorg. Chem. 40 (2001) 4040–4048.
[39] J. Ivanic, J.R. Collins, S.K. Burt, J. Phys. Chem. A 108 (2004) 2314–2323.
[40] J.S. Sears, C.D. Sherrill, J. Chem. Phys. 124 (2006) 144314.
[41] L. Cavallo, H. Jacobsen, J. Phys. Chem. A 107 (2003) 5466–5471.
[42] C. Linde, B. Akermark, P.O. Norrby, M. Svensson, J. Am. Chem. Soc. 121 (1999) 5083–5084.
[43] I.V. Khavrutskii, D.G. Musaev, K. Morokuma, Proc. Natl. Acad. Sci. U.S.A. 101 (2004) 5743–5748.
[44] J. El-Bahraoui, O. Wiest, D. Feichtinger, D.A. Plattner, Angew. Chem.-Int. Ed. 40 (2001) 2073–2076.
[45] M.C. Curet-Arana, R.Q. Snurr, L.J. Broadbelt, in: T. Oyama (Ed.), Mechanisms in Homogeneous and Heterogeneous Epoxidation Catalysis, Elsevier, Amsterdam, in press.
[46] M. Nasr-Esfahani, M. Moghadam, S. Tangestaninejad, V. Mirkhani, Bioorg. Med. Chem. Lett. 15 (2005) 3276–3278.
[47] J. Bernadou, B. Meunier, Adv. Synth. Catal. 346 (2004) 171–184.
[48] M.J. Frisch, G.W. Trucks, H.B. Schlegel, G.E. Scuseria, M.A. Robb, J.R. Cheeseman, V.G. Zakrzewski, J.A. Montgomery Jr., R.E. Stratmann, J.C. Burant, S. Dapprich, J.M. Millam, A.D. Daniels, K.N. Kudin, M.C. Strain, O. Farkas, J. Tomasi, V. Barone, M. Cossi, R. Cammi, B. Mennucci, C. Pomelli, C. Adamo, S. Clifford, J. Ochterski, G.A. Petersson, P.Y. Ayala, Q. Cui, K. Morokuma, D.K. Malick, A.D. Rabuck, K. Raghavachari, J.B. Foresman, J. Cioslowski, J.V. Ortiz, A.G. Baboul, B.B. Stefanov, G. Liu, A. Liashenko, P. Piskorz, I. Komaromi, R. Gomperts, R.L. Martin, D.J. Fox, T. Keith, M.A. Al-Laham, C.Y. Peng, A. Nanayakkara, C. Gonzalez, M. Challacombe, P.M.W. Gill, B. Johnson, W. Chen, M.W. Wong, J.L. Andres, C. Gonzalez, M. Head-Gordon, E.S. Replogle, J.A. Pople, Gaussian 98, Gaussian Inc., Pittsburgh, PA, 1998.
[49] J.P. Perdew, K. Burke, Y. Wang, Phys. Rev. B 54 (1996) 16533–16539.
[50] J.P. Perdew, Y. Wang, Phys. Rev. B 45 (1992) 13244–13249.
[51] A. Ghosh, J. Biol. Inorg. Chem. 11 (2006) 712–724.
[52] T. Matsubara, S. Sieber, K. Morokuma, Int. J. Quantum Chem. 60 (1996) 1101–1109.
[53] F. Maseras, K. Morokuma, J. Comput. Chem. 16 (1995) 1170–1179.
[54] M. Svensson, S. Humbel, R.D.J. Froese, T. Matsubara, S. Sieber, K. Morokuma, J. Phys. Chem. 100 (1996) 19357–19363.
[55] S. Humbel, S. Sieber, K. Morokuma, J. Chem. Phys. 105 (1996) 1959–1967.
[56] A.K. Rappe, C.J. Casewit, K.S. Colwell, W.A. Goddard, W.M. Skiff, J. Am. Chem. Soc. 114 (1992) 10024–10035.
[57] M. Mohr, J.P. McNamara, H. Wang, S.A. Rajeev, J. Ge, C.A. Morgado, I.H. Hillier, Faraday Discuss. 124 (2003) 413–428.
[58] M.J. Frisch, G.W. Trucks, H.B. Schlegel, G.E. Scuseria, M.A. Robb, J.R. Cheeseman, J. Montgomery, J.A.T. Vreven, K.N. Kudin, J.C. Burant, J.M. Millam, S.S. Iyengar, J. Tomasi, V. Barone, B. Mennucci, M. Cossi, G. Scalmani, N. Rega, G.A. Petersson, H. Nakatsuji, M. Hada, M. Ehara, K. Toyota, R. Fukuda, J. Hasegawa, M. Ishida, T. Nakajima, Y. Honda, O. Kitao, H. Nakai, M. Klene, X. Li, J.E. Knox, H.P. Hratchian, J.B. Cross, V. Bakken, C. Adamo, J. Jaramillo, R. Gomperts, R.E. Stratmann, O. Yazyev, A.J. Austin, R. Cammi, C. Pomelli, J.W. Ochterski, P.Y. Ayala, K. Morokuma, G.A. Voth, P. Salvador, J.J. Dannenberg, V.G. Zakrzewski, S. Dapprich, A.D. Daniels, M.C. Strain, O. Farkas, D.K. Malick, A.D. Rabuck, K. Raghavachari, J.B. Foresman, J.V. Ortiz, Q. Cui, A.G. Baboul, S. Clifford, J. Cioslowski, B.B. Stefanov, G. Liu, A. Liashenko, P. Piskorz, I. Komaromi, R.L. Martin, D.J. Fox, T. Keith, M.A. Al-Laham, C.Y. Peng, A. Nanayakkara, M. Challacombe, P.M.W. Gill, B. Johnson, W. Chen, M.W. Wong, C. Gonzalez, J.A. Pople, Gaussian 03, Gaussian Inc., Wallingford, CT, 2004.
[59] R. Seeger, J.A. Pople, J. Chem. Phys. 66 (1977) 3045–3050.
[60] R. Bauernschmitt, R. Ahlrichs, J. Chem. Phys. 104 (1996) 9047–9052.
[61] S.F. Boys, F. Bernardi, Mol. Phys. 19 (1970) 553–566.
[62] J. Krzystek, J. Telser, L.A. Pardi, D.P. Goldberg, B.M. Hoffman, L.C. Brunel, Inorg. Chem. 38 (1999) 6121–6129.
[63] A. Tulinsky, B.M.L. Chen, J. Am. Chem. Soc. 99 (1977) 3647–3651.
[64] P. Turner, M.J. Gunter, Inorg. Chem. 33 (1994) 1406–1415.
[65] K. Ayougou, E. Bill, J.M. Charnock, C.D. Garner, D. Mandon, A.X. Trautwein, R. Weiss, H. Winkler, Angew. Chem.-Int. Ed. 34 (1995) 343–346.
[66] R.S. Czernuszewicz, Y.O. Su, M.K. Stern, K.A. Macor, D. Kim, J.T. Groves, T.G. Spiro, J. Am. Chem. Soc. 110 (1988) 4158–4165.
[67] T.J. Collins, R.D. Powell, C. Slebodnick, E.S. Uffelman, J. Am. Chem. Soc. 112 (1990) 899–901.
[68] L. Cavallo, H. Jacobsen, Eur. J. Inorg. Chem. 2003 (2003) 892–902.